Pressure spectrum and structure function in homogeneous turbulence

Toshiyuki Gotoh[1] **and Daigen Fukayama**[2]
[1] *Department of Systems Engineering, Nagoya Institute of Technology, Showa-ku, Nagoya, 466-8555, Japan*
[2] *Department of Physics, Chuo University, Tokyo, 112-8551, Japan*
(Version 1.0, February 8, 2008)

The pressure spectrum and structure function in homogeneous steady turbulence of an incompressible fluid is studied using direct numerical simulation. The resolution of the simulation is up to 1024^3 and the Taylor microscale Reynolds number R_λ is between 38 and 478. The energy spectrum is found to have a small but finite inertial range followed by a bump at large wavenumbers. The Kolmogorov constant K is found to be 1.66 ± 0.08. The pressure spectrum also has a small but finite inertial range of $P(k) = B_p \bar{\epsilon}^{4/3} k^{-7/3}$ followed by a bump of nearly $k^{-5/3}$ range at higher wavenumbers. Both scaling ranges match at a crossover wavenumber, k_p, which is a characteristic wavenumber for the pressure gradient. The constant B_p is found to be about 8.34 ± 0.15 for $R_\lambda = 460$. Its non-universality is discussed. The second order pressure structure function, computed in terms of the fourth order velocity structure functions, agrees well with that obtained by the direct measurement over separations ranging between the inertial and dissipation scales.
PACS numbers: 47.27.Ak, 47.27.Jv, 47.27.Gs, 05.20.Jj

The pressure spectrum in a turbulent incompressible flow is defined as $\langle p^2 \rangle = \int_0^\infty P(k)dk$. Kolmogorov's theory predicts that

$$\begin{aligned} P(k) &= \bar{\epsilon}^{3/4} \nu^{7/4} \phi(k\eta) \\ &= B_p \bar{\epsilon}^{4/3} k^{-7/3}, \quad L^{-1} \ll k \ll \eta^{-1}, \end{aligned} \tag{1}$$

where $\phi(x)$ is a non-dimensional function, ν is the kinematic viscosity, $\bar{\epsilon}$ is the average rate of energy dissipation per unit mass, L is the integral scale of turbulence, η is the Kolmogorov scale, and B_p is a non-dimensional constant of order one. The fluid density is assumed to be unity throughout this paper.

There have been many studies of the pressure spectrum. [1–20] Some of the experiments have shown that $P(k) \propto k^{-7/3}$, [3] or equivalently $D_p = \langle (p(\boldsymbol{x}+\boldsymbol{r}) - p(\boldsymbol{x}))^2 \rangle \propto r^{4/3}$. [12,20] Others have reported that $r^{4/3}$ is not observed. [13] Recent DNS's with large scale forcing have found that the pressure spectrum is approximately proportional to $k^{-5/3}$, unlike $k^{-7/3}$, in the wavenumber range where the energy spectrum scales close to $k^{-5/3}$. [16–18] Gotoh and Rogallo conjectured that the observed $k^{-5/3}$ scaling for $P(k)$ is a bump, as observed for the energy spectrum, and that $P(k)$ scales as $k^{-7/3}$ in the lower wavenumber range. This implies that a wider inertial range, compared to the energy spectrum, is necessary for K41 scaling of $P(k)$. [18] There seems to be no agreement about the scaling of the pressure spectrum when compared to the case of the energy spectrum.

We have performed a series of DNS's of incompressible homogeneous isotropic turbulence using a resolution of up to $N = 1024^3$. The DNS was designed to generate a wider inertial range and higher Reynolds numbers. The range of the Taylor microscale Reynolds number $R_\lambda = \bar{u}\lambda/\nu$ is between 38 and 478, where $\bar{u}$ is the root mean square of turbulent velocity and λ is the Taylor microscale. The characteristic parameters of the DNS are listed in Table I. The code uses the pseudo Fourier spectrum and 4th order Runge Kutta Gill methods. Random forcing, Gaussian and white in time, is applied to the lower wavenumbers. A statistically steady state was confirmed by observing the time evolution of the total energy, the total enstrophy and the skewness of the longitudinal velocity derivative. The statistical averages were taken as the time average over tens of turnover times for lower Reynolds numbers and over a few turnover times for the higher Reynolds numbers. The data of the highest Reynolds number, $R_\lambda = 478$, were obtained as short time average (about 0.34 eddy turnover times) during the passage toward steady state rather than over a statistically steady state. The resolution condition $k_{max}\eta > 1$ is satisfied for most runs, but that of the case when $R_\lambda = 460$ is slightly less than unity. We believe that this does not adversely affect the energy and pressure spectra results in the inertial range. Computations with $R_\lambda \le 284$ were performed using a Fujitsu VPP700E vector parallel machine with 16 processors at RIKEN. Simulations using higher R_λ were performed on a Fujitsu VPP5000/56 with 32 processors at the Nagoya University Computation Center.

The energy spectra in Kolmogorov units (multiplied by $(k\eta)^{5/3}$) are shown in Fig.1. Collapse of curves at various Reynolds numbers is very satisfactory, although the curves with $R_\lambda \ge 284$ have appreciable rise of $E(k)$ near the high wavenumber boundary. The Kolmogorov constant K was measured in the range of $0.008 \le k\eta \le 0.04$ in which the average energy transfer flux function $\Pi(k)/\bar{\epsilon}$ is nearly flat and close to unity (figure not shown). The value of K

$$K = 1.66 \pm 0.08, \tag{2}$$

is very close to the value of 1.62 obtained in previous experiments and DNS's, [21,22] and to the value of 1.72 obtained using the Lagrangian spectral theory (LRA). [23,24] There is a small spectral bump at wavenumbers near $k\eta \approx 0.2$, as observed in other DNS's. [22]

Figure 2 shows the pressure spectra in terms of the K41 scaling, Eq.[1], multiplied by $(k\eta)^{7/3}$ for various Reynolds numbers. Fig. 3 is a close-up of the curves for higher Reynolds numbers. For $R_\lambda < 300$ there is no plateau in the curves. However, for R_λ larger than 400, there appears to be a small plateau of finite length. There is a bump, with a peak value of about 17, in $P(k)$ near $k\eta = 0.2$ which is more appreciable than that in the energy spectrum. The left part of the bump consists of a finite ramp. For $R_\lambda = 284$, the slope of the ramp is close to 2/3, indicating that $P(k) \propto k^{-5/3}$. The slope gradually decreases as the Reynolds number increases. It is this part which the previous DNS's have observed as $P(k) \propto k^{-5/3}$. [16–18]

The curves obtained for $R_\lambda = 387$, 460 and 478 indicate that $P(k)$ approaches the $k^{-7/3}$ spectrum over the range of $0.008 < k\eta < 0.04$. The value B_p is

$$B_p = 8.34 \pm 0.15, \tag{3}$$

shown in Fig.3 as a horizontal line. Taking into account the relatively short length of the averaging time, the error bar for B_p is a few times larger than 0.15. Pullin obtained $B_p = 1.325K^2$ using the joint Gaussian hypothesis for the 4th order velocity structure functions. With $K = 1.66$, $B_p = 3.65$, which is smaller than the present DNS value. This is consistent with the fact that $P(k)$ is larger than $P_G(k)$, computed from the Gaussian random velocity field with the same energy spectrum as that of the actual turbulence field. [5,6,18] Pumir suggested $B_p \approx 7$ using DNS data with $N = 128^3$ at $R_\lambda = 77.5$. Pullin estimated that $B_p \approx 2.14 - 3.65$ using Lundgren's stretched spiral vortex model.

The collapse of the $P(k)$ curves for all R_λ's is not as good as the energy spectrum, even in the dissipation range. The collapse of the pressure spectra is improved when the normalized pressure gradient variance, $F_{\nabla p} = \langle(\nabla p)^2\rangle\bar{\epsilon}^{-3/2}\nu^{1/2}$, is included in the scaling for $P(k)$:

$$P(k) = F_{\nabla p}\bar{\epsilon}^{3/4}\nu^{7/4}\phi_1(k\eta), \tag{4}$$

where $\phi_1(x)$ is a non-dimensional function. [19,25] Figure 4 presents $P(k)$ using Eq.[4], and clearly shows that the scaling of $P(k)$ in the high wavenumber range is better than the scaling using Eq.[1]. The inset shows the variation of $F_{\nabla p}$ against the Reynolds number. $F_{\nabla p}$ is a monotonically increasing function of R_λ that becomes very weakly dependent on R_λ as R_λ becomes large. It should be noted that although the insensitivity of $F_{\nabla p}$ to R_λ is consistent with Batchelor's Gaussian theory for the pressure, its value is considerably larger than the value corresponding to the Gaussian theory, $F^G_{\nabla p}$. [1,18] This insensitivity of $F_{\nabla p}$ at large R_λ implies that the collapse of $P(k)$ with $R_\lambda \geq 284$ is little affected by $F_{\nabla p}$. However, there still remains a weak Reynolds number dependence of $P(k)$ in the inertial range, causing the pressure spectrum to be non-universal. Close inspection of $P(k)$ in the $k^{-7/3}$ range shows that the factor $F_{\nabla p}$ of Eq.[4] improves the collapse of the curves (Figs. 2 and 4). In this range, $\phi_1(k\eta) = C_p(k\eta)^{-7/3}$, where C_p is a non-dimensional constant of the order one. The constant B_p is related as $B_p = F_{\nabla p}C_p$, so that B_p becomes weakly dependent on Reynolds number, while C_p is not. It is reasonable, in this sense, to regard C_p as a more universal constant than B_p. Using the values of B_p and $F_{\nabla p}$ we obtain

$$C_p = 0.707 \pm 0.1. \tag{5}$$

The non-universality enters the pressure spectrum through $F_{\nabla p}(R_\lambda)$ as a function of R_λ. Therefore, $F_{\nabla p}$ is a key parameter for the second order statistics of pressure. The Reynolds number dependence of $F_{\nabla p}$ is attributed to the coherent structure of the source term field in the Poisson equation for the pressure. [18,25]

Transition to the nearly $k^{-5/3}$ range occurs at $k\eta \approx 0.03$ for $R_\lambda \geq 387$, which corresponds to $k_p\lambda_p \approx 1.5, 1.8$ and 1.6 for $R_\lambda = 387, 460$ and 478, respectively. Here, λ_p is a characteristic length scale for the pressure gradient defined by $\langle(\partial p/\partial x)^2\rangle = \bar{u}^4/\lambda_p^2$. This is analogous to the Taylor microscale. Thus the crossover scale between the $k^{-7/3}$ and the nearly $k^{-5/3}$ ranges is about $k_p = \lambda_p^{-1}$.

The pressure spectrum at low wavenumbers scales as

$$P(k) = \bar{\epsilon}^{4/3}L^{7/3}\phi_2(kL), \tag{6}$$

where L is the integral scale. The curves of $P(k)$ at this range collapse reasonably well into one curve (figure not shown). The scaling of Eq.[4] matches Eq.[6] in the $k^{-7/3}$ range.

Hill and Wilczak have derived an expression for the pressure structure function $D_p(r)$ in terms of the fourth order velocity structure functions, assuming a homogenous and isotropic velocity field:

$$\begin{aligned} D_p(r) = -\frac{1}{3}L(r) + \frac{4}{3}r^2\int_r^\infty y^{-3}[L(y) + T(y) - 6M(y)]dy \\ + \frac{4}{3}\int_0^r y^{-1}[T(y) - 3M(y)]dy, \end{aligned} \tag{7}$$

where $L(r) = \langle\delta u(r)^4\rangle, T(r) = \langle\delta v(r)^4\rangle$, $M(r) = \langle\delta u(r)^2\delta v(r)^2\rangle$, and $\delta u(r)$ and $\delta v(r)$ are the longitudinal and transversal velocity differences, respectively. [10]

Isotropy has been examined in terms of the kinematic conditions for the second and third order moments of the longitudinal and transversal velocity increments. The relations are well satisfied for both $R_\lambda = 387$ and $R_\lambda = 460$.

(The relative error in the equation for the third order moments is less than about 10% at $r/\eta = 200$.)

Figure 5 shows plots of $L(r), T(r)$ and $M(r)$ at $R_\lambda = 387$ and 460. There is a straight line contained along each curve between $50 < r/\eta < 400$. The straight line showes the slope of 1.28, the value predicted by She and Lévêque. [27] An examination of the local exponent of the curves showed that the inertial range exponents defined by $L(r) \propto r^{\zeta_4^L}, T(r) \propto r^{\zeta_4^T}$ and $M(r) \propto r^{\zeta_4^M}$ have plateau between $90 < r/\eta < 200$ and $1.24 < \zeta_4^T < \zeta_4^M < \zeta_4^L < 1.32$ for $R_\lambda = 460$. [20] The detailed analysis will be reported elsewhere. [26]

$D_p(r)$ computed by Eq.[7] is compared with values obtained using direct measurement in Fig. 6. The curves for $R_\lambda = 460$ are shifted upward by one unit for clarity. Agreement of the curves for $r/\eta < 150$ is satisfactory. It is reasonable to expect that the isotropy of the fourth order velocity structure functions in the limit of $r \to 0$, the fundamental assumption for the derivation of [7], is well satisfied. The pressure gradient variance and the pressure structure function at small separations can be examined in terms of Eq.[7]. [10,20] In the inset of Fig.4, the values of $F_{\nabla p}$ computed using $D_p(r)r^{-2}$ in the limit of $r \to 0$ are found to be very close to the value of $F_{\nabla p}$ obtained by direct measurement.

The straight line in Fig.6 indicates the r^1 slope. The slope of $D_p(r)$ is very close to unity and between 2/3 and 4/3. The scaling of $D_p(r)$ requires a much longer scale separation than the case using wavenumber space.

The authors acknowledge Profs. Antonia and Nakano for their helpful discussions, and express their thanks to Nagoya University Computation Center and the Advanced Computing Center at RIKEN for providing the computational resources. This work was supported by a Grant-in-Aid for Scientific Research (C-2 12640118) by The Ministry of Education, Science, Sports and Culture of Japan. T.G's work was supported by the "Research for the Future" Program of the Japan Society for the Promotion of Science, under the project JSPS-RFTF97P01101.

[1] G. K. Batchelor, Proc. Camb. Phil. Soc. **47**, 359 (1951).
[2] A. S. Monin and A. M. Yaglom, *Statistical Fluid Mechanics* (MIT, Cambridge, MA 1975) Vol. 2.
[3] W. K. George, P. D. Beuther and R. E. A. Arndt, J. Fluid Mech. **148**, 155 (1984).
[4] M. Holzer and E. Siggia, Phys. Fluids A **5**, 2525 (1993).
[5] T. Gotoh and R. S. Rogallo, *Proc. of the Summer Program,* Center for Turbulence Research, Stanford University and NASA Ames Research Center, 189 (1994).
[6] D. I. Pullin and R. S. Rogallo, *Proc. of the Summer Program,* Center for Turbulence Research, Stanford University and NASA Ames Research Center, 177 (1994).
[7] A. Pumir, Phys. Fluids **6**, 2071 (1994).
[8] M. Nelkin, Advances in Phys. **43**, 143 (1994).
[9] D. I. Pullin, Phys. Fluids **7**, 849 (1995).
[10] R. J. Hill and J. M. Wilczak, J. Fluid Mech. **296**, 247 (1995).
[11] R. J. Hill, Phys. Fluids **8**, 3085 (1996).
[12] M. Ould-Rouis, R. A. Antonia, Y. Zhu and F. Anselmet, Phys. Rev. Lett. **77** 2222, (1996).
[13] R. J. Hill and O. N. Boratav, Phys. Rev. E **56**, R2363 (1997).
[14] R. J. Hill and S. T. Thoroddsen, Phys. Rev. E **55**, 1600 (1997).
[15] G. A. Voth, K. Satyanarayan and E. Bodenschatz, Phys. Fluids, **10** 2268 (1998).
[16] P. Vedula and P. K. Yeung, Phys. Fluids **11**, 1208 (1999).
[17] N. Cao, S. Chen and G. D. Doolen, Phys. Fluids **11**, 2235 (1999).
[18] T. Gotoh and R. S. Rogallo, J. Fluid Mech. **396**, 257 (1999).
[19] T. Gotoh and K. Nagaya *Proceedings of IUTAM Symposium on Geometry and Statistics of Turbulence.* ed. by Kambe (Kluwer 1999)
[20] B. R. Pearson and R. A. Antonia, submitted to J. Fluid Mech. (2000).
[21] K. R. Sreenivasan, Phys. Fluids. **7**, 2778 (1995).
[22] P. K. Yeung and Y. Zhou, Phys. Rev. E **56**, 1746 (1997).
[23] Y. Kaneda, J. Fluid Mech. **107**, 131 (1981).
[24] Y. Kaneda, Phys. Fluids. **29**, 701 (1986).
[25] T. Gotoh, K. Nagaya and S. Wada, submitted to J. Phys. Soc. Japan. (2000).
[26] R. Kerr, M. Meneguzzi and T. Gotoh, submitted to Phys. Fluids. (2000).
[27] Z. S. She and E. Lévêque, Phys. Rev. Lett. **72**, 336 (1994).

TABLE I. DNS parameters and Statistical quantities of runs: T_{eddy}^{av} is the length of time average.

R_λ	N	$k_{max}\eta$	ν	c_f	forcing range	T_{eddy}^{av}	E	ϵ	L	λ	λ_p	$\eta(\times 10^{-2})$	$F_{\nabla p}$	K	B_p
38	128^3	60	1.50×10^{-2}	1.30	$\sqrt{3} \le k \le \sqrt{12}$	22.6	1.99	1.19	0.891	0.501	0.371	4.10	3.62	-	-
70	256^3	121	4.00×10^{-3}	0.50	$\sqrt{3} \le k \le \sqrt{12}$	49.7	1.16	0.457	0.785	0.318	0.256	1.93	5.60	-	-
125	512^3	241	1.35×10^{-3}	0.50	$\sqrt{3} \le k \le \sqrt{12}$	5.52	1.25	0.492	0.744	0.185	0.170	0.841	7.61	-	-
284	512^3	241	6.00×10^{-4}	0.50	$1 \le k \le \sqrt{6}$	3.03	1.96	0.530	1.246	0.149	0.177	0.449	10.4	1.64	-
387	1024^3	483	2.80×10^{-4}	0.51	$1 \le k \le \sqrt{6}$	1.09	1.81	0.522	1.215	0.0986	0.131	0.255	11.3	1.62	-
460	1024^3	483	2.00×10^{-4}	0.51	$1 \le k \le \sqrt{6}$	1.43	1.79	0.506	1.150	0.0841	0.119	0.199	11.8	1.64	8.48
478	1024^3	483	2.80×10^{-4}	0.51	$1 \le k \le \sqrt{6}$	0.34	2.00	0.419	1.350	0.116	0.142	0.269	11.8	1.74	8.19

Fig.1 Scaled energy spectra, $\bar{\epsilon}^{-1/4}\nu^{-5/4}(k\eta)^{5/3}E(k)$. $K = 1.66 \pm 0.08$.

Fig.2 K41 scaling for the pressure spectra, $\bar{\epsilon}^{-3/4}\nu^{-7/4}$ $(k\eta)^{7/3}P(k)$.

Fig.3 Close up of $\bar{\epsilon}^{-3/4}\nu^{-7/4}(k\eta)^{7/3}P(k)$ for higher Reynolds numbers. A short straight line shows the slope of $k^{2/3}$ and a horizontal line indicates $B_p = 8.34$.

Fig.4 Scaling of the pressure spectra with the factor $F_{\nabla p}$, $F_{\nabla p}^{-1}\bar{\epsilon}^{-3/4}\nu^{-7/4}$ $(k\eta)^{7/3}P(k)$. The lines are the same as those in Fig. 2. The inset is the variation of $F_{\nabla p}$ against R_λ. Squares are $F_{\nabla p}$ computed by $\lim_{r\to 0} D_p(r)/r^2$, and other symbols are experimental data by Voth *et al.* [15]

Fig.5 Fourth order structure functions of velocity increments. $R_\lambda = 387$ and $R_\lambda = 460$ (thick lines). A straight line shows the slope of 1.28.

Fig.6 Comparison of $D_p(r)$ with H & W. [10] $R_\lambda = 387$ and $R_\lambda = 460$ (thick lines). A straight line shows the slope of r^1. The curves for $R_\lambda = 460$ are shifted upward by one unit for clarity.

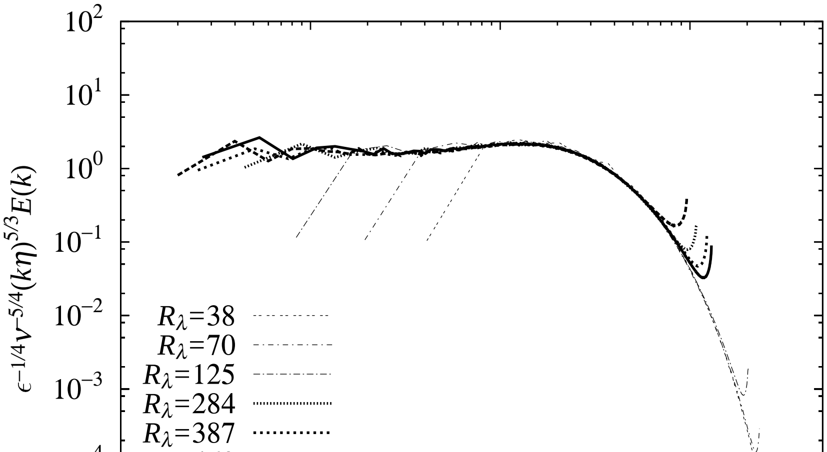

10^2
10^1
10^0
10^{-1}
10^{-2}
10^{-3}
10^{-4}
10^{-5}
$\epsilon^{-1/4}\nu^{-5/4}(k\eta)^{5/3}E(k)$
0.001
0.01
0.1
1
$k\eta$
R_λ=38
R_λ=70
R_λ=125
R_λ=284
R_λ=387
R_λ=460
R_λ=478

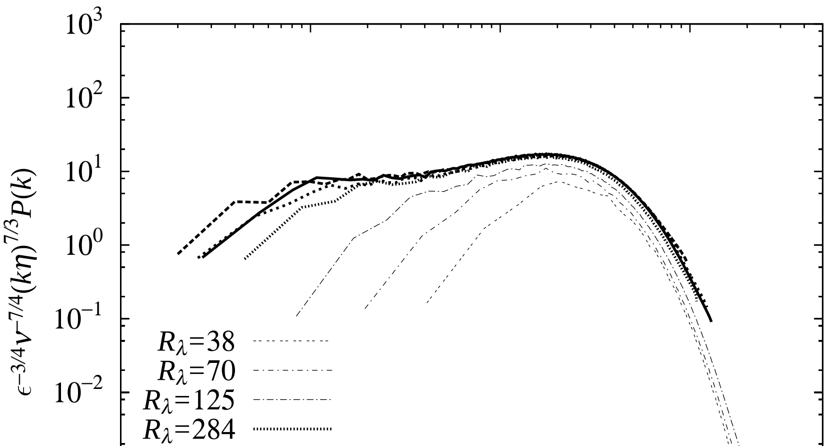

10^3
10^2
10^1
10^0
10^{-1}
10^{-2}
10^{-3}
10^{-4}
$\epsilon^{-3/4}\nu^{-7/4}(k\eta)^{7/3}P(k)$
0.001
0.01
0.1
1
$k\eta$
R_λ=38
R_λ=70
R_λ=125
R_λ=284
R_λ=387
R_λ=460
R_λ=478

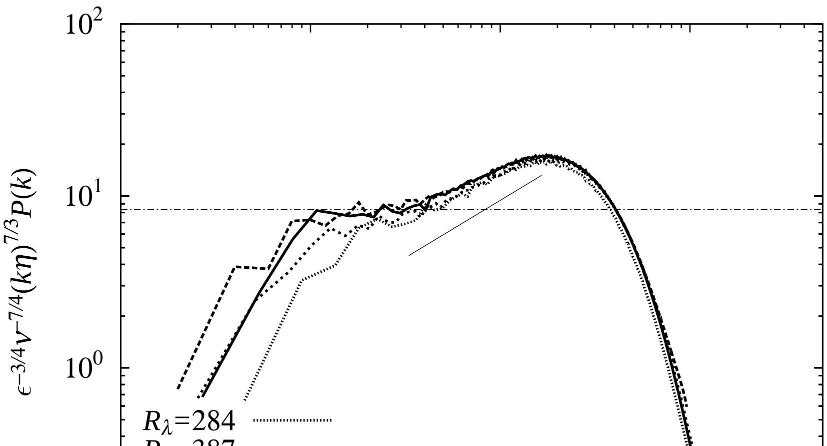

10^2
10^1
10^0
10^{-1}
0.001
0.01
0.1
1
$k\eta$
$\epsilon^{-3/4}\nu^{-7/4}(k\eta)^{7/3}P(k)$
R_λ=284
R_λ=387
R_λ=460
R_λ=478

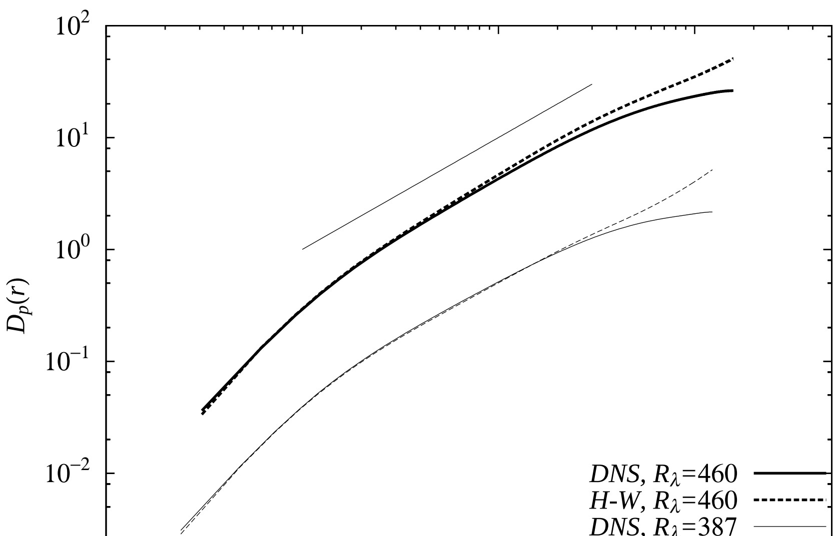

10^2
10^1
10^0
10^{-1}
10^{-2}
10^{-3}
$D_p(r)$
1
10
100
1000
r/η
DNS, R_λ=460
H-W, R_λ=460
DNS, R_λ=387
H-W, R_λ=387

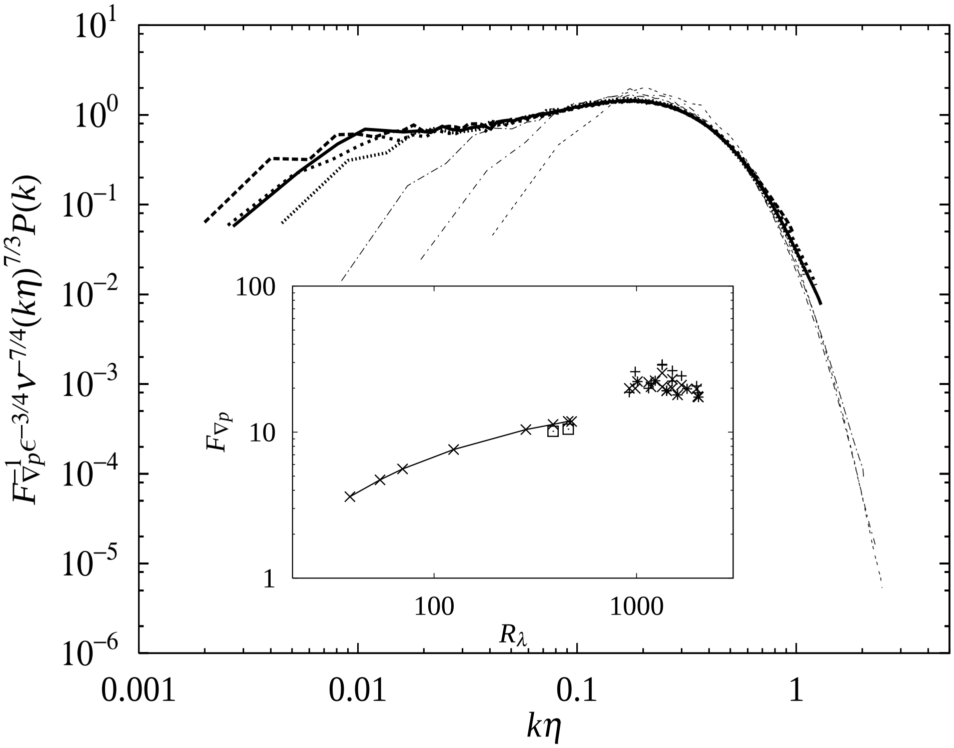

10^{1}
10^{0}
10^{-1}
10^{-2}
10^{-3}
10^{-4}
10^{-5}
10^{-6}
$F_{\nabla p}^{-1}\epsilon^{-3/4}\nu^{-7/4}(k\eta)^{7/3}P(k)$
0.001
0.01
0.1
1
$k\eta$
100
10
1
$F_{\nabla p}$
100
1000
R_λ

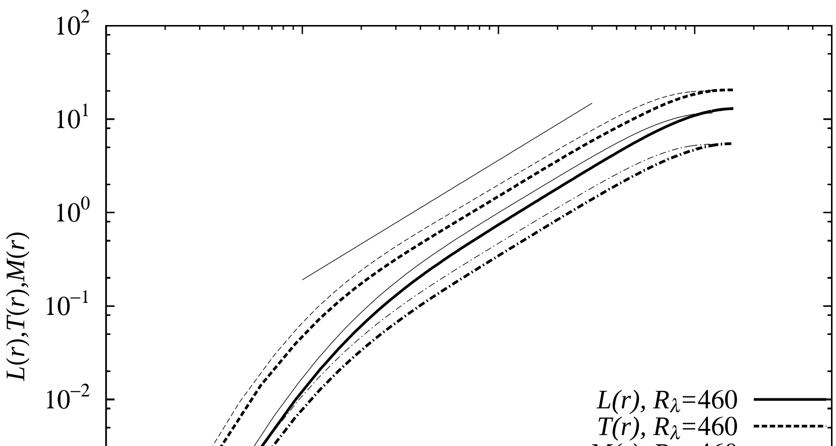

10^{2}
10^{1}
10^{0}
10^{-1}
10^{-2}
10^{-3}
10^{-4}
1
10
100
1000
r/η
$L(r),T(r),M(r)$
$L(r)$, R_λ=460
$T(r)$, R_λ=460
$M(r)$, R_λ=460
$L(r)$, R_λ=387
$T(r)$, R_λ=387
$M(r)$, R_λ=387